Journal of Biomechanical Science and Engineering

Vol. 4, No. 1, 2009

An Un-Momentous Start to Life: Can Hydrodynamics Explain Why Fish Larvae Change Swimming Style?*

Ulrike K MÜLLER**, Johan L van LEEUWEN***, Stephan van DUIN*** and Hao LIU****

**Department of Biology, California State University Fresno
2555 E San Ramon Avenue, Fresno CA 93740, USA
E-mail:umuller@csufresno.edu
*** Experimental Zoology Group, Wageningen University
Marijkeweg 40, 6709 PG Wageningen, The Netherlands
**** Graduate School of Engineering, Chiba University
1-33 Yayoi-cho, Inage-ku, Chiba, 263-8522 Japan

Abstract

In this study, we explore mechanical constraints on the swimming performance of zebrafish larvae (*Danio rerio*) that might explain why larvae switch from sustained swimming to the more efficient burst & coast as they grow. Two hypotheses have been proposed to explain why young fish larvae perform poorly at burst & coast. First, their initial momentum might be low; second, their drag coefficient might be high. To test the two hypotheses, this study makes a quantitative comparison between experimental observations of swimming fish larvae and a CFD model of a self-propelled fish. The study focuses on larvae of the crucial age and size range in which zebrafish switch swimming style. Our studies show that hatchlings perform poorly not only because they cannot accelerate to a high initial coasting speed and hence do not gain enough initial momentum. But they also suffer higher decelerations while coasting due to a high drag coefficient. Overall, the fivefold difference in coasting distance between hatchlings and older larvae corresponds closely to a threefold difference in the time constant of the speed decay and a threefold difference in initial momentum. Our data also show that swimming speed does not decay exponentially, as predicted by the drag-speed relationship in the viscous flow regime, but hyperbolically, due to flow phenomena developing in the boundary layer during the coast.

Key words: Burst and Coast, Intermittent Swimming, Zebrafish, *Danio Rerio*, Fish Larvae, Viscous Flow Regime

1. Introduction

Intermittent swimming and hydrodynamic scaling.

Fish rarely swim steadily and instead use intermittent swimming — the fish executes a few tail beats during the burst phase and then coasts for a considerable distance, keeping its body more or less straight. Intermittent locomotion has several possible advantages over sustained swimming. While sustained swimming may be powered by red slow-twitch muscle alone, these muscles have a lower power output than white fast-twitch muscles. Therefore higher swimming speeds require the fish to recruit its anaerobic white muscles, which work more efficiently when used in short bursts at their optimal contraction

*Received 11 July, 2008 (No. 08-0465)
[DOI: 10.1299/jbse.4.37]

frequency rather than continuously at a lower frequency [1,2]. Intermittent swimming might also reduce costs associated with the higher drag incurred during undulatory swimming, particularly at low speeds [3]. Therefore, intermittent swimming might be most effective when the drag acting on a coasting fish is considerably lower than the drag acting on a bursting fish.

The asymmetry between drag during the burst *versus* during the coast depends on flow regime. Flow regime affects the ratio of pressure drag to viscous drag, the two main forces that make up the total drag acting on a swimming fish. Viscous drag depends on the fish's surface area, which is essentially the same during the burst and during the coast phase. Pressure drag depends on the fish's frontal area, which is higher during the burst phase because the fish's lateral body undulations increase its frontal area. Viscous drag D_{vis} is proportional to swimming speed U and body length L [4]:

$$D_{vis} \approx LU;\ D_{vis} = C_{vis}\, L\mu U \qquad (1)$$

while pressure drag D_{pres} increases with the square of swimming speed and the fish's frontal area A [5]:

$$D_{pres} \approx AU^2;\ D_{pres} = C_{pres}\, A\, \tfrac{1}{2}\, \rho U^2 \qquad (2)$$

Intermittent swimming might therefore not be profitable for organisms swimming in the viscous flow regime, when viscous drag dominates over pressure drag and therefore an asymmetry in the 'burst' drag versus 'coast' drag is unlikely. When fish larvae hatch, their body length of a few millimeters [6] and low swimming speeds [7,8,9] put hatchlings in the intermediate flow regime, in which both viscous and pressure drag play important roles [10,11]. Larval drag forces might therefore scale with speed at an exponent intermediate between 1 and 2, confounded by the ontogenetic changes in body shape and body length. During their development, as the larvae grow and swim faster, they gradually shift to the inertial flow regime of their parents. This shift in flow regime might increase the profitability of intermittent swimming.

Two ways to maximize coast distance.

Intermittent swimming is most effective if the fish can coast over long distances, thereby reducing the distance covered and time spent swimming actively. So, the fish should quickly accelerate and then coast with a very gradual loss of forward speed. In the viscous flow regime, drag is proportional to swimming speed and hence the coasting speed $U(t)$ should decay exponentially over the duration t of the coast:

$$U(t) = U_0\, e^{-t/\tau} \qquad (3)$$

with U_0 being initial coasting speed and τ the time constant of the exponential decay (= time when $U(t) = U_0/e$). Therefore, coasting distance x can be described by:

$$x(t) = U_0\, \tau\, (1 - e^{-t/\tau}) \qquad (4)$$

In order to maximize coasting distance, a given fish can either increase its initial coasting speed U_0 or increase the time constant τ of the speed decay.

In the inertial flow regime, drag is proportional to the square of speed and therefore the swimming speed decreases according to a hyperbolic decay function:

$$U(t) = \frac{U_0}{\left(\frac{U_0}{\kappa}\right)t + 1} \qquad (5)$$

with a distance constant κ (= distance covered when $U(t) = U_0/e$). Integrating eq. 5 for our particular case of a coasting fish shows that in the inertial flow regime, coasting distance x is no longer directly proportional to the distance constant κ and initial coasting speed U_0:

$$x(t) = \kappa \ln\left[\left(\frac{U_0}{\kappa}\right)t + 1\right] \tag{6}$$

The speed U_0 to which the fish can accelerate is limited by muscle power, propulsive force, and the total drag acting on the undulating body. Maximum speed is reached when propulsive power equals power dissipation due to drag. Fish can also increase their coast distance by reducing drag during the coast phase and thereby increasing τ.

Ontogeny of burst & coast swimming: two hypotheses.

While most adult fish favor burst-and-coast swimming, fish larvae initially swim cyclicly and only switch to burst & coast swimming as they grow older [12]. Intermittent swimming requires fast acceleration during the burst phase and slow deceleration during the coast. Fast acceleration during the burst phase requires that the fish can generate substantially more thrust than drag. Slow deceleration requires that the drag on the coasting fish is low. Fish larvae can accelerate up to considerable steady swimming speeds during their extended escape responses [9,13], which shows that fish larvae can burst. However, early fish larvae seem to do poorly at coasting and hence strictly speaking cannot burst & coast. Two hypotheses have been formulated about the scaling of the burst & coast performance during larval development. One hypothesis focuses on the coast phase [14], and the fact that the distance covered during the coast is inversely proportional to the drag acting on the larva. The other hypothesis focus on the burst phase[11], and the fact that coast distance depends on the momentum gained by the larva during the burst phase.

The first hypothesis argues from a 'hydrodynamic scaling of drag' point of view. As long as viscous drag dominates the total drag acting on the body, intermittent swimming offers no energetic benefits. Furthermore, a previous study on the hydrodynamic scaling of coasting performance in fish has shown that smaller fish decelerate faster than larger fish, which suggests that smaller fish have higher drag coefficients [11,15]. So, flow regime and hydrodynamic scaling of drag seem to favor larger fish. Weihs [14] predicted that burst & coast swimming becomes attractive as fish larvae grow fast and long enough to enter the inertial flow regime. Weihs puts the critical Reynolds number for the transition from viscous to inertial flow regime at around 10, based on evidence from bluff bodies. His analytical model of larval swimming, based on observations of anchovy larvae [12], showed that fish larvae switch to burst & coast at the same critical body length as the length at which they exceed Reynolds numbers of 10 during routine swimming. Hence, hydrodynamic scaling of drag forces might explain the switch in swimming style. However, observations on swimming fish larvae suggest that this transition from viscous to inertial flow regime might occur later at Reynolds numbers around 300 [10], weakening the flow-regime aspect of the 'hydrodynamic scaling' hypothesis.

The second hypothesis argues that the ability to achieve sufficiently high initial coasting speeds best explains ontogenetic changes in coasting performance [11]. McHenry and Lauder [11] explored the hydrodynamic scaling of drag on zebrafish larvae experimentally, confirming the flow regime transition at Reynolds numbers around 300 and thereby weakening the first hypothesis on hydrodynamic scaling. Furthermore, they found that differences in coasting performance with age were best explained not by hydrodynamic scaling effects on body drag, but by differences in initial coasting speed between smaller and larger fish. They measured coasting performance in zebrafish ranging in age from 5

days post-fertilization to adult. At age 5 days, zebrafish larvae have made the transition from steady to intermittent swimming. The 'momentum' hypothesis has therefore not yet been tested concerning the switch in larval swimming style.

The present study.

The present study focuses on the critical size range when the transition from sustained to burst & coast swimming occurs in zebrafish. When they hatch, zebrafish larvae are 3.0 to 3.5 mm long and swim cyclicly at speeds up to 60 Ls^{-1} [7,9]. However, within a few days after hatching, burst & coast becomes the dominant swimming style. On the one hand, this switch might be driven by physical constraints on the coast phase ('hydrodynamic scaling' hypothesis); the drag acting on the larva might change due to a change in flow regime or due to ontogenetic events, such as the absorption of the yolk-sac. Both these 'hydrodynamic scaling' arguments focus on changes in the decay constant τ as driving force for the change in swimming style. On the other hand, the switch in larval swimming style might also be driven by an increase in initial coasting speed ('momentum' hypothesis), which in turn might be due to a lower body drag or an increase in thrust due to a larger muscle power output. We explore the following questions: (1) how does coasting performance change with age around the switch from steady to intermittent swimming, (2) how do pressure and viscous drag change with age around this switch in swimming style, and finally (3) can the changes in coasting performance be explained better by the momentum or the hydrodynamic scaling hypothesis?

2. Material & Methods

Fish.

Zebrafish (*Danio rerio* Hamilton 1822) larvae were reared in the laboratory from wild-type parents. Eggs and larvae were held in batches of ca. 50 individuals in 1-liter jars filled with aerated water at 28°C. The jars were inspected daily, and egg shells and debris were removed manually; the water was replaced every 2–3 days. The rearing temperature was kept at a constant 28°C by half submerging the jars in a large tank filled with temperature-controlled water placed in a temperature-controlled room. The eggs and larvae were maintained at a 12h:12h light:dark cycle. The larvae were fed *Paramecium* (at 4 and 5 days post-fertilization) twice a day. For our experiments, we used sibling larvae 2, 3, 4, and 5·days post-fertilization (dpf).

To calculate momentum and Reynolds number, we determined larval body mass and body length for all 4 age groups (Table 1). Larval body length increased from 3.2 to 4.3 mm and larval body mass increased from 3.2 to 4.3 mg.

Kinematics recordings of coasting performance.

Experiments took place in a temperature-controlled room (room temperature 30°C), keeping the water temperature at 28°C. Ten sibling larvae were transferred to ten Petri dishes (diameter 10 cm, water depth 1 cm) and one dish after another was placed on the stand of a dissection microscope for uniform illumination. We elicited escape responses (by touching the larva with a hair) to record coast behavior in 2 and 3 dpf old larvae, which do not yet swim spontaneously. The 4 and 5 dpf old larvae often swam spontaneously, so fewer of the recorded bouts are escape responses. We recorded 5 to 10 swimming bouts per larva for 10 larvae for all four age groups (2, 3, 4, and 5 dpf), collecting data for a total of 180 swimming bouts. We filmed top views through a Nikon Macro lens (105 mm Nikkor Micro 1:2.8; Tokyo, Japan) with a digital high-speed camera (Photron APX RS; Japan; recording at 1000 frames per second at an exposure time of 1/3000 s and a resolution of 1024×1024

pixels). In all analyzed images, we did not observe surface waves. The larvae initiate bursts usually on the bottom of the Petri dish. During the burst phase, they rise to the middle of the water column and then sink back to the bottom after the coast phase.

Kinematic analysis.

From the kinematic recordings, we extracted initial coasting speed and coasting distance. The beginning of the coasting phase was defined as the moment when the total curvature along the body's central axis was less than 10 L^{-1}, which occurred when the tail tip had reached a position approximately half way between maximal lateral excursion of the last tail beat and the mean path of motion. To find this threshold value of the midline curvature, we automatically tracked the outlines of the fish larvae and digitized 10 points on the central axis of the outline using Matlab 7.0 (MathWorks, Inc., Natick, MA, USA). These raw midlines were interpolated and smoothed in space and time using a cubic spline fit to obtain 51 equidistant points along the fish's central axis [9,16,17]. We then calculated the integral of the instantaneous local curvature along the posterior body (from 0.75 to 1.0L) to determine the moment when total curvature of the central axis (calculated as the integral of the local curvature and normalized by larval body length) had dropped below 10 L^{-1}. The swimming speed at that moment was defined as initial coasting speed U_0. We then tracked the position of the fish through time and space for up to 200 ms to determine coasting distance.

To test the momentum hypothesis, we calculated initial momentum from the fish's initial coasting speed and the average body mass of its age group. We then fit the relationship between coasting distance and momentum for each age group with a linear regression (reduced major axis) and compared the slopes of these regression lines (unpaired Tukey test and Student t test). We also calculated one global regression line for all data points (reduced major axis) and calculated the residuals for each age group to assess by how much any given age group deviated from the overall performance and tested whether any age-group averaged residuals are significantly different from zero (unpaired Tukey test).

To test the hydrodynamic scaling hypothesis, we also determined the time constant of the speed decay during the coast. From this decay constant we then determined initial deceleration, drag and drag coefficient. We determined the decay constant in two ways, first assuming a viscous flow regime, and hence an exponential decay of coasting speed over time (eq. 3). To this end, we first normalized instantaneous coasting speed by initial coasting speed and then fit an exponential decay function (eq. 3) to the combined data sets of normalized speed over time for a given age group. Fitting a single exponential function over the entire coasting period poorly predicts the initial speed decay, which indicates that the speed decay is probably not a single exponential decay. We therefore used only the first 100 ms of all coasting episodes for the fit to predict the time constant τ. To account for the fact that speed does not decay to 0 within 100ms, we fit the decay function with an offset and minimized the error by optimizing offset and time constant τ. In the second fitting procedure, we assumed an inertial flow regime and fit therefore a hyperbolic-decay function (eq. 5) to the normalized speed decay data. In this way, we derived a second set of initial decelerations, drags and drag coefficients. This experimental drag coefficient is calculated based on equation 1.

Flow recordings of coasting behavior.

To record the flow patterns generated during coasting behavior, five to ten sibling larvae were transferred to a small filming tank (inner dimensions 50 by 50 mm; water level 10 mm; water temperature 27°C) 2 to 4 hours after the last feeding period and allowed to acclimate for half an hour. The water was seeded with small Nylon beads (Degussa Vestosint; diameter 6 μm; density 1016 kg m^{-3}; seeding density 0.04 to 0.05 $pixel^{-1}$ or 5 000

to 6 000 particles mm^{-3}). Flow fields were recorded with a high-speed digital camera (Redlake MotionPro, San Diego, CA, USA; 800 frames·s^{-1}, 1280 by 640, exposure time 250 μs) and a macro lens (105·mm Nikon Micro 1:2.8, f stop 5.6, with a 27.5·mm extension ring) mounted above the aquarium. The long axis of the field of view was 8.3·mm. We used a 400 mm (focal length) plano-convex lens and 63 mm (focal length) plano-cylindrical lens to generate a light sheet from the beam of a continuous Argon ion laser (max. power 2 Watt, Coherent Innova 90). In the filming area, the light sheet was 25 mm wide and 0.2 mm thick. The light sheet was situated 2 to 3 mm below the glass lid of the film tank. All recorded swimming behavior was either spontaneous or a response to the presence of the other larvae. We recorded 10 coasting sequences in total for age groups 3, 4, 5 dpf, of which we fully analyzed one sequence per age group.

PIV analysis.

We selected three sequences for complete kinematic plus PIV analysis, in which the fish coasts horizontally in the light sheet – sequences with a non-horizontal swimming path were used only for qualitative comparison to test consistency of drawn conclusions. We used a super-PIV routine[18], embedded in a custom Matlab 7.0 program to batch-process sequences of up to 300 frames[19]. The size of the initial sub-image for the DPIV's correlation procedure was 32^2 pixels, and reduced to 16^2 for the second and final correlation. The fish was not masked, so the PIV correlation routine included pixels that comprise the fish, which reduces accuracy of the flow information adjacent to the fish. In the recorded sequences, the width of the fish's posterior body corresponded to 30 pixels at its widest point behind the yolk-sac.

CFD model.

An *in-house* CFD-based simulator was established to model self-propelled fish and biomimetic-robot swimming. This versatile simulator integrates the modeling of realistic morphologies, complex kinematics, and unsteady hydrodynamics. The morphological model was built using a differential geometry-based method and a grid generator for fins and body; in order to let complex geometries perform equally complex flapping and undulating movements, their geometry is modeled using a multi-block and overset grids method. The undulating body motions were captured by a kinematic model that can mimic realistic fin-body-kinematics; an analytical method combined with multi-coordinate systems is employed for dynamic grid regeneration. An FVM-based NS solver for highly deformable multi-block and overset grids systems was verified to be self-consistent[21,22]; and an integrated method of estimating propulsive energetics was established which calculates inertial and hydrodynamic forces, powers and propulsive efficiency. Moreover a dynamic model was coupled with the CFD-based simulator, which is capable of analyzing the dynamics of maneuvers for a freely swimming locomotor.

To build the geometric model for this study, we digitized the larval body shape. From dorsal and lateral photographs, we determined the height and width of the larval body, finfold, eyes and yolk-sac at 51 points along the larval body axis. This yielded a geometric description of the larval body, finfold, eyes and yolk-sac as a sequence of up to 50 elliptical disks whose thickness corresponds to 2% of the total larval body length. We quantified the shape of 5 larvae per age group and used the data of the larva closest to the mean value of all 5 larva of one age group. These shape data are then used by a grid generator [20] to build simultaneously the three-dimensional geometric wireframe model plus the computational grid. To build the kinematic model, we used an image sequence of a larva swimming cyclicly [9,17] and reduced tail beat amplitude gradually to 0 over the duration of three tail beats. By coupling a swimming dynamic model with the present CFD model, we built a burst-cyclic-coast kinematic model that executes self-propelled free-swimming. Hence, we

can obtain instantaneous pressure and viscous drags over the duration of the coast as well as instantaneous swimming speed and coasting distance. The computational time domain is six tail beat cycles long: the larva executes four tail beat cycles before it begins to coast for the duration of two tail beat cycles. The spatial computational domain is four body lengths long and four body heights wide and high.

To define the Reynolds number (*Re*) and reduced frequency, we used the initial coasting speed as reference speed and the body length as reference length; the calculated *Re* are listed in Table 2. From the CFD model, we derived values for the drag coefficient, based on equation 2.

3. Results

Burst and coast behavior.

Hatchling zebrafish (age 2 dpf) rarely swim spontaneously; when kept in a group of 10 larvae, hatchlings and 3-dpf old larvae more often exhibit cyclic rather than burst-and-coast swimming (**Fig. 1**). Cyclic swimming can also be elicited by the experimenter as part of an extended escape response. We use the term 'cyclic' to indicate swimming bouts in which the larva uses a wide body wave to maintain a constant mean swimming speed above 5 Ls^{-1} for more than 5 tail beats [9]. Larvae aged 2 and 3 dpf also execute burst-type spontaneous swimming bouts with a narrow body wave amplitude[9], which take place very close to the bottom of the Petri dish and usually result in little or no net displacement even during the active phase of the swimming bout. We therefore evaluated mainly coasting episodes that resulted from escape responses elicited by the experimenter, in which the 2 and 3 dpf old larva swims higher in the water column: of 88 recorded swimming bouts, 70 are escape responses. At age 4 dpf, zebrafish larvae begin to feed and to swim spontaneously in the water column in a burst-and-coast style. Of the 92 recordings of age group 4 and 5 dpf, only 20 are escape responses.

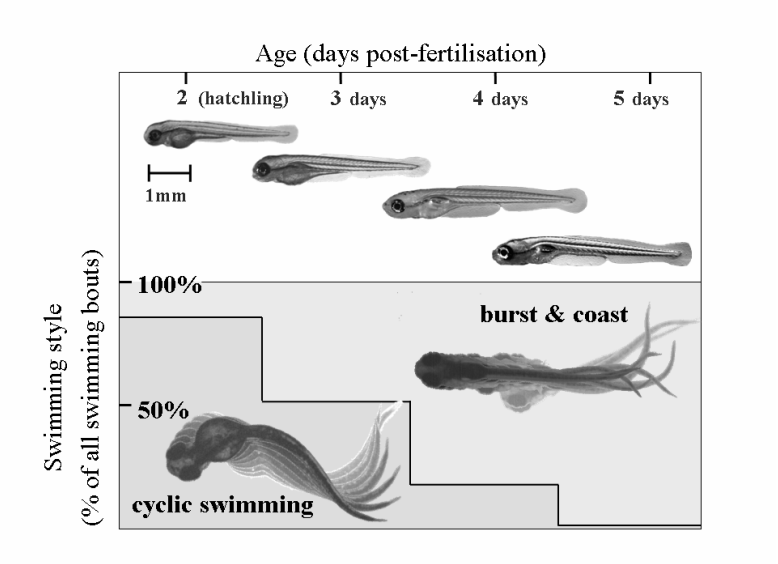

Fig. 1: Relative frequency of bouts of cyclic and burst & coast swimming in zebrafish larvae aged 2 to 5 days post-fertilization (dpf). Top panel: lateral views of larvae aged 2 to 5 dpf. Bottom panel: proportion of cyclic swimming decreases with age; overlaid on the bottom panel: top views of a 2-day old larva during a cyclic swimming bout and a 4-day old larva during a burst-and-coast bout.

A swimming bout consists of a propulsive phase when the lava is beating its tail and a non-propulsive phase when the larva is coasting. The recorded swimming bouts (burst +

coast phase) last between 0.25 and 1.5 seconds. We included 93 of 180 recorded coasts in this study; we selected those sequences in which (1) the larva initiated the coast in the water column, (2) the larva was not beating its pectoral fins while coasting, (3) the larva maintained its body posture and did not roll during the coast, and (4) the larval body straightened during the coast to a total curvature along the body of less than $5L^{-1}$. Hatchlings, but not the older larvae, occasionally roll during the burst phase.

Fish larvae reduce mainly tail beat amplitude and to a lesser extend tail beat frequency over several tail beats of the active swimming phase (**Fig. 2**). Tail beat frequency drops by one third during the last three tail beat cycles from 44±17 to 30±5 Hz (n = 93) in all four age groups, while tail beat amplitude is reduced to zero by the end of the last tail beat. We defined the onset of coasting based on curvature of the body's central axis, normalized by larval body length.

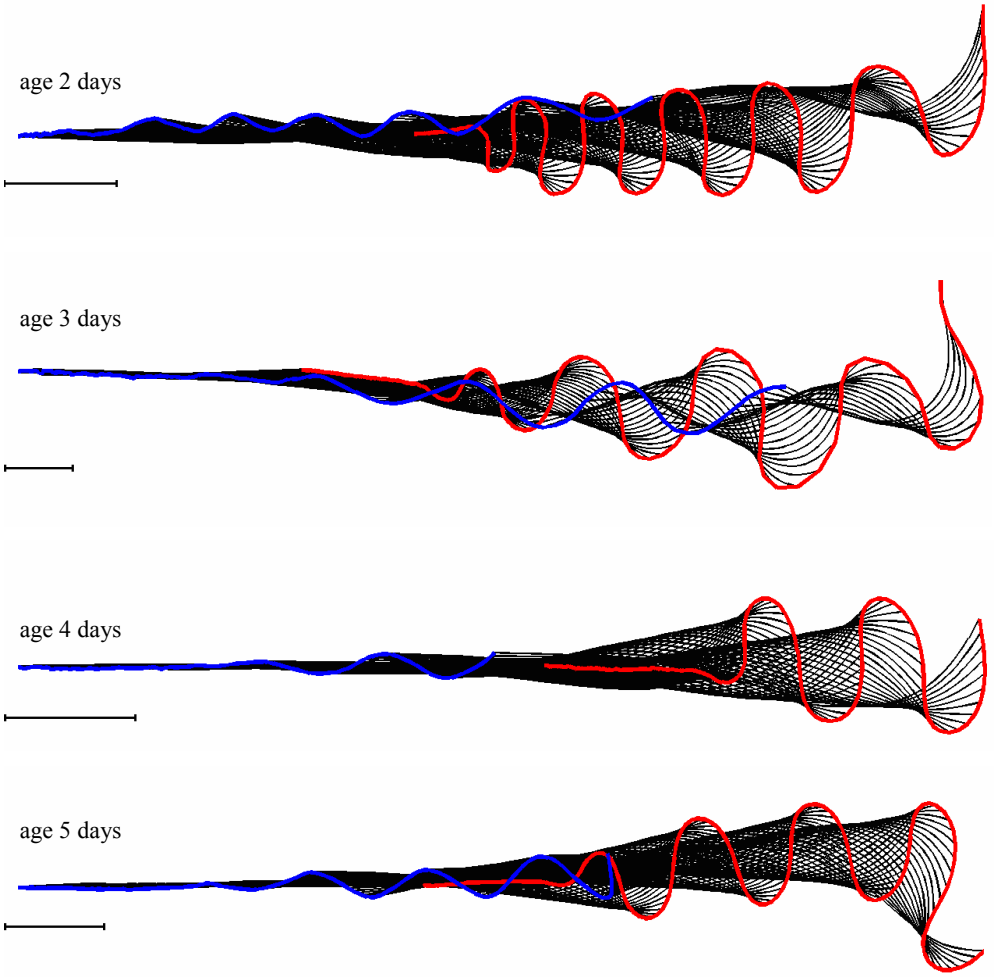

Fig. 2. Motion pattern of a zebrafish during the transition from burst to coast. Shown are superimposed midlines (black) for up to six tail beats of active swimming and the entire coast phase. The time separation between individual midlines is 2 ms. Red line: path of the tail tip; Blue line: path of the snout. Scale bar corresponds to 1 mm.

How coasting performance changes with larval age.

The duration of the coast phase is very variable in fish larvae, ranging from 1.32 to 0.12 seconds, with an average duration of 0.45±0.24 s (N=93). Due to this large variation within each age group, coast duration does not change systematically with age: the correlation between age and coast duration was not statistically significant (r^2 = 0.002).

However, there are significant differences in the distance covered (**Fig. 3**) (**Table 1**). Hatchlings underperform significantly in coasting distance ($P<0.001$; unpaired Student's t-test): older larvae coast up to four times further than hatchlings. This difference persists when coasting distance is scaled by body length. Hatchlings coast over a distance of less than 10% of their body length, whereas larvae 3 to 5 dpf old coast over a distance of 20 to 40% of their body length, up to four times as far as hatchlings.

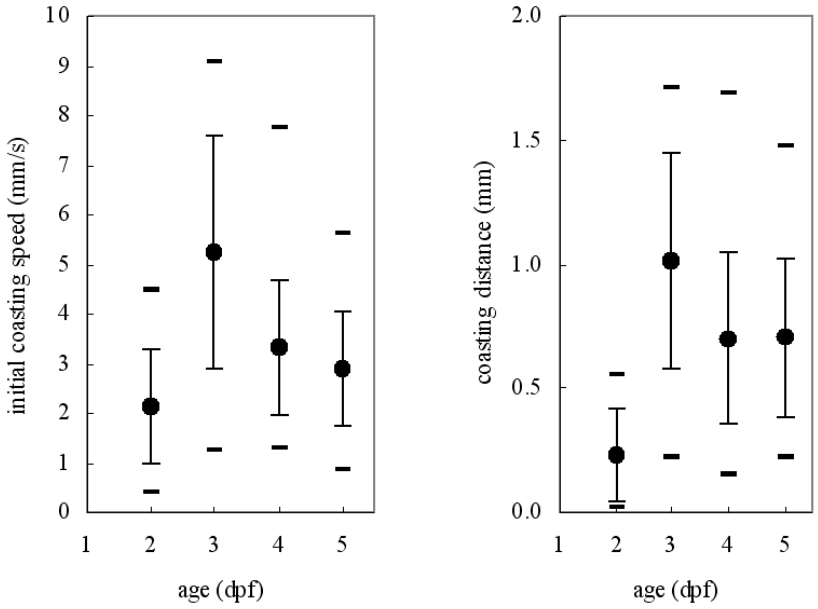

Fig. 3. Initial coasting speed (left) and coasting distance (right) of zebrafish larvae aged 2 to 5 days post-fertilization. Shown are mean value (●) ± standard deviation, smallest and largest value (–).

Hatchling zebrafish start coasting at half the initial swimming speed U_0 compared with older larvae, despite 90% of the analyzed swimming bouts being escape responses vs. 76% in 3-day old larvae and 16% in the 4- and 5-day larvae (**Table 1**). Initial swimming speed varies widely within each age group, the standard deviation of each age-specific mean is in the order of half the mean value (37 to 54%), but variation decreases with age (**Table 1**). These observations are consistent with the expectation that younger larvae have a lower and less consistent coast performance than older larvae. The mean initial speed is highest (5.2±2.4 mms^{-1}, N=25) at 3 dpf, when 75% of the evaluated sequences are escape responses.

Table 1. Morphological characteristics and coasting performance of zebrafish larvae aged 2 to 5 days post-fertilization. Sample size N on all morphological data is 100. Otherwise N is given in brackets. Time constant $\tau_{(t100)}$ is given for the exponential fit over the first 100 ms only.

Age (days)	Body length (mm)	Body mass (mg)	Total coasting duration (ms)	Total coasting distance (mm)	Initial coasting speed (mm/s)	Time constant $\tau_{(t100)}$ (ms)
2	3.20±0.14	3.2±0.14	174±105 (21)	0.26±0.23 (21)	2.1±1.1 (21)	25±1 (10)
3	3.44±0.17	3.4±0.17	357±320 (21)	1.37±0.81 (21)	5.2±2.3 (21)	53±2 (21)
4	4.19±0.15	3.8±0.15	317±168 (32)	0.94±0.57 (32)	3.3±1.5 (32)	39±1 (32)
5	4.27±0.14	4.3±0.14	341±197 (23)	0.96±0.43 (24)	2.9±1.1 (25)	80±2 (25)

Hatchlings not only have a lower initial speed, their coasting speed also drops faster. Hatchling coasting speed drops to half its initial value within 30 ms. In older larvae, this decay is slower, with coasting speed dropping to half its initial value within 50 to 80 ms. So hatchlings have twice to four times lower time constants τ than older larvae (**Table 1**).

Momentum and coasting performance.

Differences in coasting distance between age groups might be due to differences in initial momentum. Our measurements show that hatchlings have the lowest body mass (**Table 1**) and initial coasting speeds (**Fig. 3**), and therefore have the lowest momentum. The highest average momentum was observed in 3-day old larvae – they have the highest initial coasting speeds (**Table 1**).

When fitting a linear regression to the relationship between momentum and coasting distance for all larvae, we find a close correlation with a high coefficient of determination (r^2 =0.94) (reduced major axis regression). The regressions for each age group show that the slope for the hatchling age group is significantly lower than the slope through the total data set and the age-specific regression slopes for the other three age groups – for a given momentum, older larvae tend to coast further than hatchlings (**Fig. 4**). This observation suggests that hatchlings might experience a higher deceleration than older larvae. To quantify this underperformance, we calculated residuals based on the perpendicular offset from the combined linear-regression line. If an age group is represented fairly by the combined regression line, then their residuals should be not significantly different from zero. This is true of all older larvae, but not the hatchlings. Hatchlings significantly underperform (**Fig. 4**) ($p < 0.001$; Tukey test and unpaired student T-test): Their mean residual is -0.077 (±0.095, n = 20), which translates into a coasting distance that is 29% shorter than that of older larvae at the same initial coasting speed.

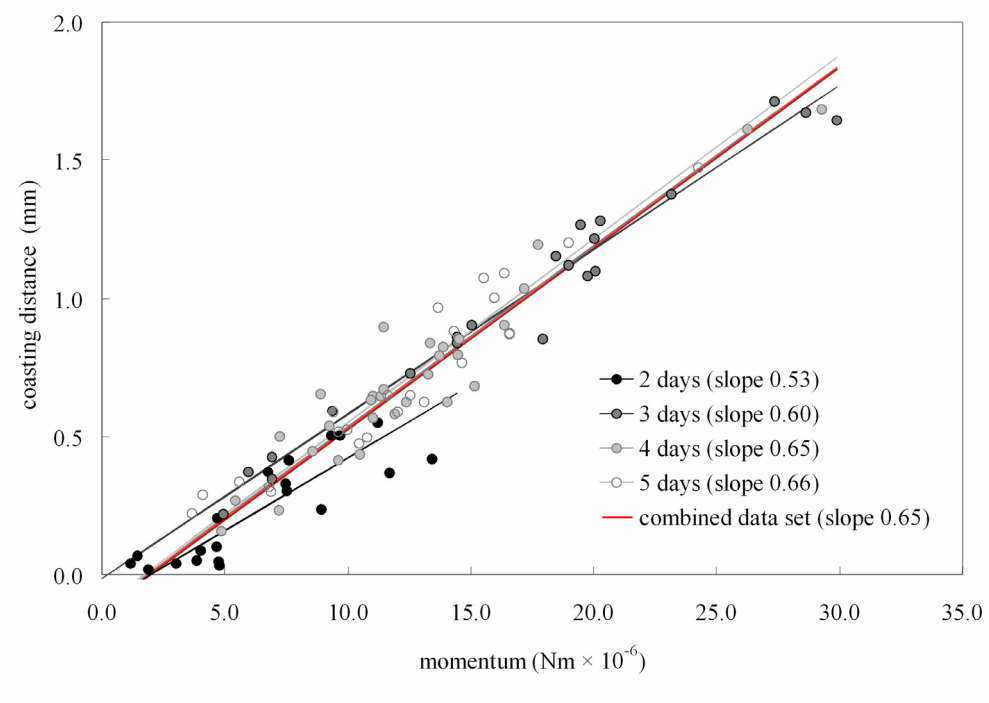

Fig. 4. Relationship between coasting distance and momentum for zebrafish larvae aged 2 to 5 days post-fertilization. The graph shows regression fits to the data from each age group (grey) and to the combined data set (red); the slopes of each regression line is given in brackets in the legend.

In summary, momentum explains 94% of the overall variation in the coasting distance of early zebrafish larvae, but not necessarily 94% of the actual performance. Coasting distance is proportional to initial momentum in the viscous flow regime. So, if momentum determines coasting distance, then an up to 5.2-fold range in coasting distances over the observed age range must correspond to the same range in momentum. Yet, we observe only a factor 1.2 to 2.3 difference in initial coast speed, and a factor 1.1 to 1.3 difference in mass, which amounts to an up to 2.6-fold range in momentum. So, despite a strong correlation between coasting distance and momentum, the range in momentum is considerably smaller than the range in coasting distance, suggesting that other factors might contribute more strongly to the differences in coasting performance between hatchlings and older larvae.

Drag and coasting performance.

We expected that coasting distance should be proportional to initial momentum and the time constant of the speed decay. Hence the up to five-fold increase in costing distance should also correspond to similar increases in momentum and time constant. Our observations of coasting larvae yield time constants τ that range from 25 ms for hatchlings to 80 ms for 5-day old larvae (**Table 1**). So, τ increases by a factor of 1.6 to 3.3 over our examined age range. This relative increase in τ is similar to the increase in momentum by a factor of 1.8 to 2.6. So both factors –an increase in initial coasting speed and a decrease of coasting drag– contribute to the improved coasting performance of older larvae.

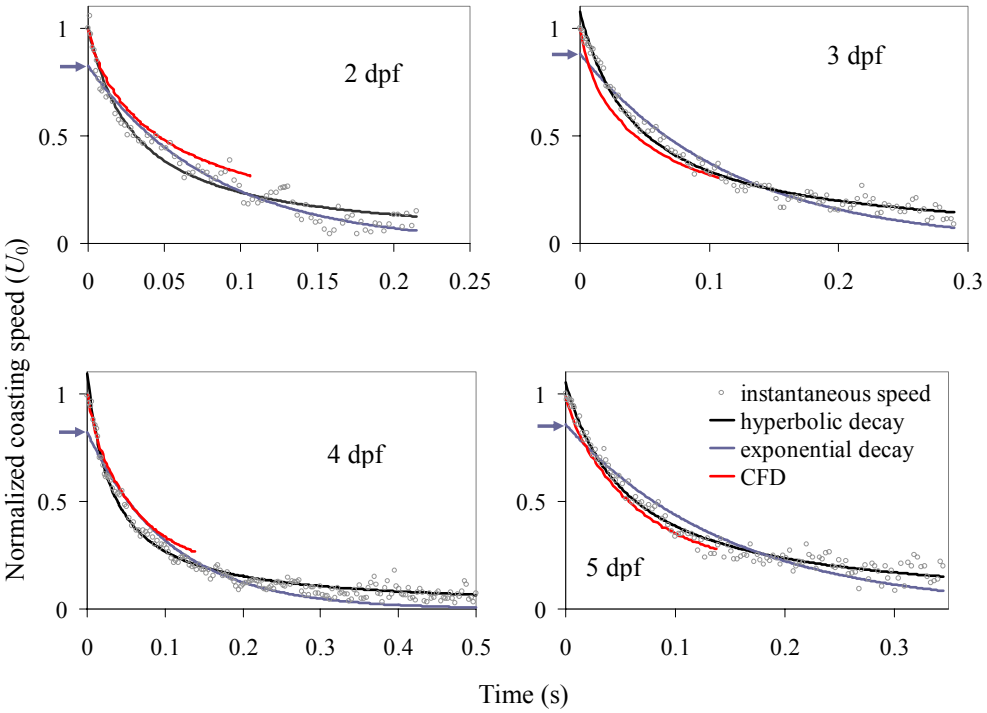

Fig. 5. Decay in coasting speed for zebrafish larvae aged 2 to 5 days post-fertilization. Shown are every third data point of the original data from 10 larvae per age group, the hyperbolic (black) and exponential (blue) function fit to the data, and the decay modeled by CFD (red). The blue arrow on the Y axis indicates U_0 of the exponential fit.

Our experiments yield estimates for drag and drag coefficients, which have been used to assess the flow regime of coasting fish [11]. We estimated initial deceleration by fitting an exponential decay function (eq. 3, viscous flow regime) and a hyperbolic decay function (eq. 5, inertial flow regime). The hyperbolic functions fit the observed speed decay more closely than the exponential decay function (**Fig. 5**) for the older larvae, but not the hatchlings. For

all age groups, the exponential fit is particularly poor for the steep speed decay during the first few milliseconds of the coast phase. So, we use the deceleration values from the hyperbolic decay function to calculate initial drag and drag coefficient (**Table 2**).

The fact that a hyperbolic decay function fits our observed speed decay better than an exponential decay function, does not imply that larvae coast in an inertial flow regime. At low Reynolds numbers, flow regime cannot be gleaned from the nature of the decay function because the underlying assumption is not valid that the sum of body mass and virtual mass of a decelerating body is approximately constant. Because the virtual mass of the coasting larva changes, coasting speed does not decay as a single exponential function. This effect can be seen in our CFD and flow visualization data in the next sections in the form of boundary layer phenomena that lower viscous drag.

Table 2. Values for drag estimated from experimental and CFD data for zebrafish at time t = 0 ms of the coasting period.

Age (days)	Larval surface area (mm^2)	Larval frontal area (mm^2)	Reynolds number at t_0	Initial total drag at t_0 (±2.5 ms) based on experiments (μN)	Initial total drag at t_0 (±2.5 ms) based on CFD (μN)	Drag coefficient at t_0 based on experiment C_{exp}	Drag coefficient at t_0 based on CFD C_{CFD}
2	8.4	0.28	7	21(18-25)	16	10.2	2.1
3	10.4	0.30	17	39(37-46)	50	6.6	0.9
4	12.6	0.24	14	40(37-50)	36	7.6	1.2
5	12.3	0.25	12	22(21-25)	29	4.1	1.2

Drag estimates from our recorded coasting episodes yield initial drag values of 21 to 40 μN. Our CFD simulation yield very similar values ranging from 16 to 50 μN. Drag drops very steeply at the beginning of the coast due to the steep drop in speed, and therefore the experimental drag values are very sensitive to t_0. In a time window of ±2.5 ms around t_0, our experimental drag estimates range from 18 to 50 μN.

The drag coefficients based on the drag values from the observed coasting behavior show that hatchlings generate relatively more drag than older larvae – their drag coefficient is the highest at 10 (**Table 2**). Older larvae have lower drag values between 4 and 8. The CFD results show a similar picture – hatchlings have the highest drag coefficient of 2.1 while older larvae have drag coefficients between 0.9 and 1.2 (**Table 2**). So, after removing size and speed effects, our results show that hatchlings are hampered in their coasting by their relatively higher drag compared with older larvae.

Our decay data show that the CFD model fits the measured data well over the computed time period of 100 to 140 ms (**Fig. 5**). The CFD model shows that during active swimming and at the initiation of the coast, viscous forces contribute at least 89% to the total force in all age groups (**Fig. 6**). The high viscous contribution to the total drag indicates that fish larvae swim in the viscous flow regime. As coasting speed plummets during the first 50 ms of the coast, so do total and viscous drag (**Fig. 6**). This drop is almost entirely due to the drop in viscous drag; despite the rapid drop in coasting speed, pressure drag remains above 50% of its active-swimming value during the first 50 ms of the coasting phase (**Fig. 6**).

Over the duration of the coast (we calculated values for up to 140 ms of coasting), the ratio of viscous to pressure drag drops from a value of 8.5 to 1.2 (**Fig. 6**). This decrease in the contribution of viscous drag is caused by water in the fish's boundary layer overtaking the coasting fish. Our flow visualization experiments show that the larva decelerates faster than the surrounding water that is initially dragged along with the larva. This difference in

deceleration causes the water adjacent to the larva to move forward faster than the larva, which reduces the viscous drag on the larva (**Fig. 7**). We observed this flow effect in all examined age groups. This decrease in viscous drag is the most likely explanation for the fact that coasting speed is not modeled well by a single exponential decay function.

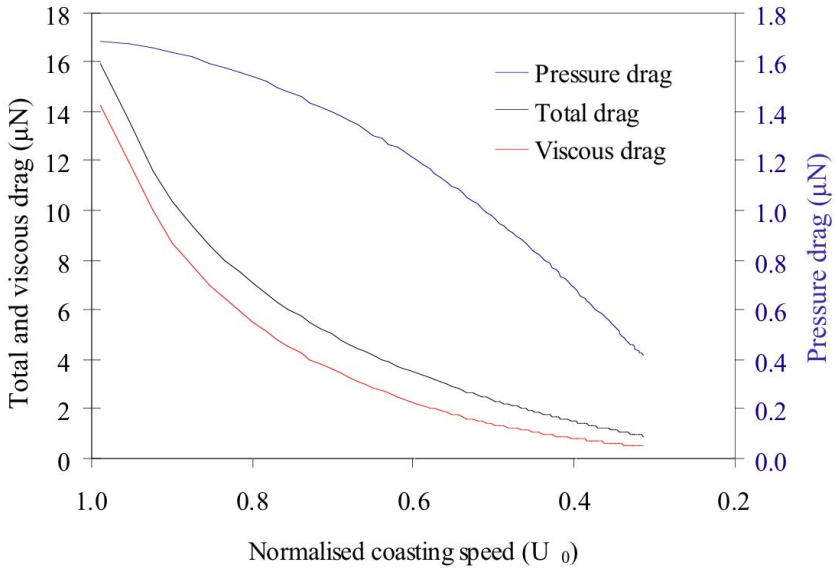

Fig. 6. Decay of the drag acting on a 2-day old zebrafish larva according to our CFD model. Shown are total, viscous, and pressure drag decay as a function of normalized coasting speed (= instantaneous speed / initial coasting speed). Note that pressure drag (right Y axis) is an order of magnitude smaller than total drag (left Y axis).

Flow patterns around coasting larvae.

The CFD flow fields are in good agreement with the observed flow fields (**Figs. 7,8**).

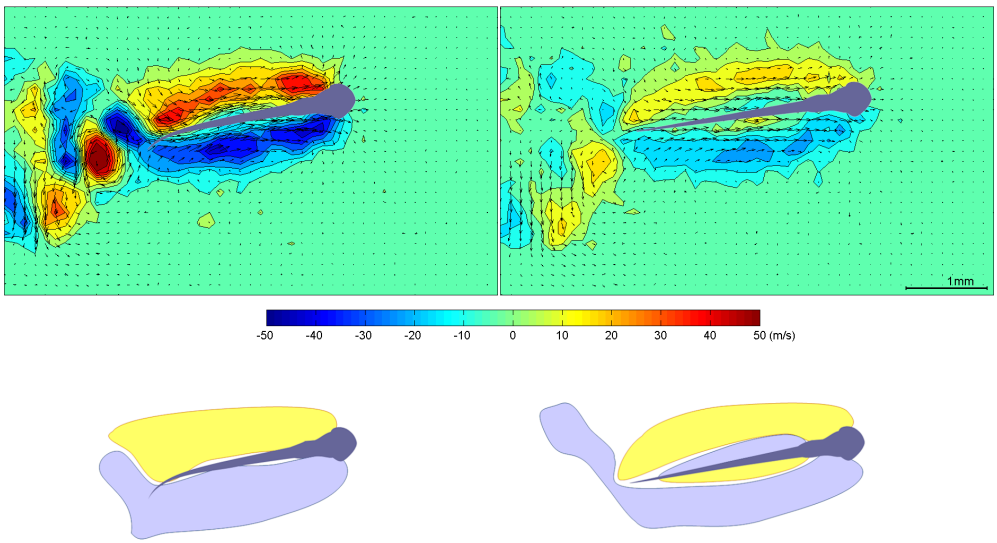

Fig. 7. Top panel. Vorticity fields of coasting larva (age 3 days post-fertilization) at the initiation of the coast (t = 0 ms) and at time t = 25 ms. The color map indicates vorticity (m s^{-1}). The vorticity near the body changes sign during the first third of the coasting phase as water adjacent to the larva begins to overtake the fish. Bottom panel. Sketch of the boundary vorticity to illustrate the sign reversal of the boundary vorticity near the larva's body.

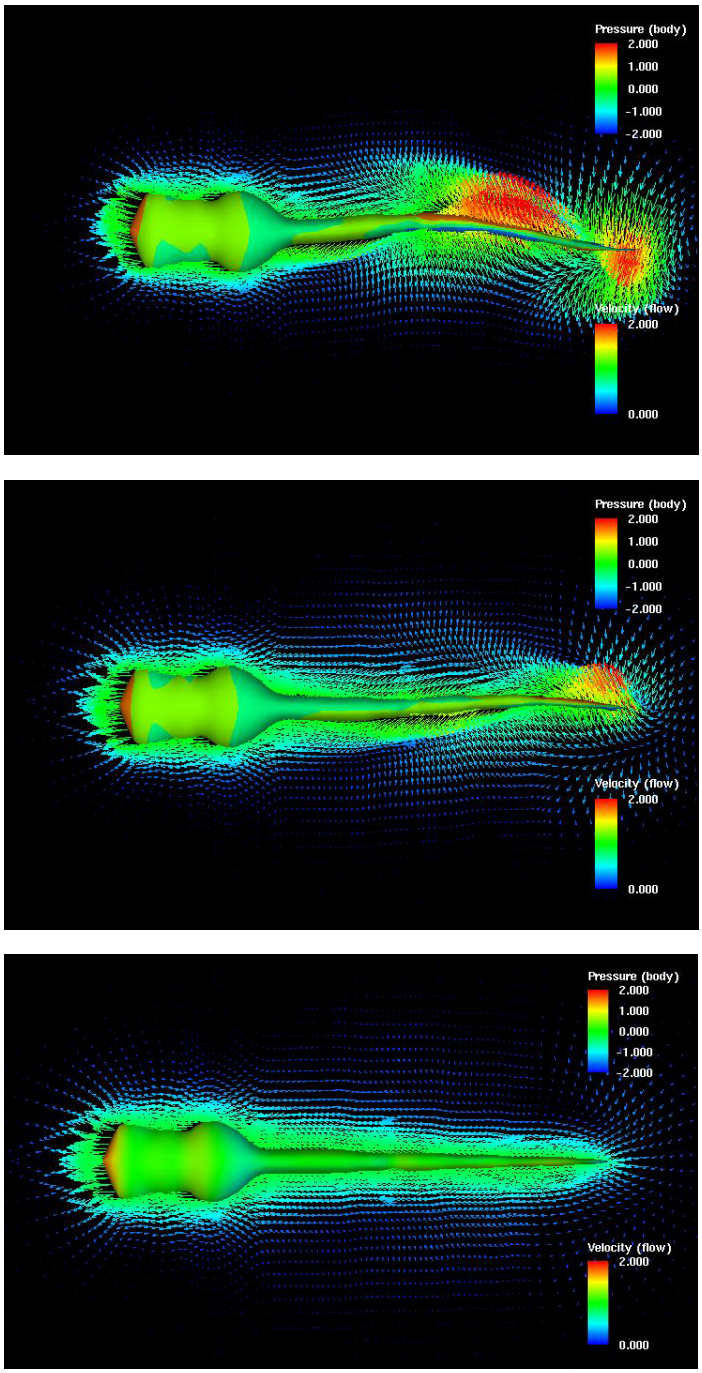

Fig. 8. Computed flow fields around a zebrafish larva (age 2 days post-fertilization) immediately before and after the initiation of the coast. The time separation between sequential images is 8 ms. The color-coded arrows indicate non-dimensionalized flow velocity (normalized by initial coasting speed U_0). The color on the larval body indicates the distribution of non-dimensionalized pressure.

While the larva is still undulating its body, the flow adjacent to the undulating sections of the body is oriented mainly laterally. But the drag wake is already evident immediately adjacent and behind the yolk-sac. As the larva begins to coast, all flow velocity vectors near the larva align themselves with the larval body and point in the coasting direction of the larva – the drag wake has enveloped the entire larva.

At the beginning of the coast, the larva develops a boundary layer that is accelerated

by the coasting larva and that quickly grows wider than the larval body (**Fig. 8**). Yet, within the first 100 ms of the coast, the larva slows down faster than its boundary layer until the inner sections of the boundary layer move forward faster than the larva. This reversal of relative speed results in a new boundary layer building up near the larva with an opposite sense of rotation to the outer parts of the boundary layer, as evident in our PIV data (**Fig. 8**) and our CFD simulation (not shown). This reversal is most likely an inertial phenomenon.

4. Conclusions

Momentum hypothesis.

Our first question was how coasting performance changes with age. Our experiments show that zebrafish larvae coast further as they get older because they have a higher initial momentum. We find an up to fivefold increase in coasting distance over a less than threefold increase in momentum, lending support to the momentum hypothesis. Momentum increases with age mainly due to an increase in initial coasting speed: Older fish larvae might achieve higher initial coasting speeds because they achieve higher tail beat frequencies [9], which leads to higher accelerations. Higher tail beat frequencies imply that older larvae can contract their muscles faster and generate more muscle power.

Hydrodynamic scaling hypothesis.

Differences in momentum however do not explain the poor coasting performance of hatchlings. Hatchlings have a higher drag coefficient than older larvae and consequently their coasting speed decays more than three times faster than older larvae. The higher drag coefficient might be caused by the combination of its relatively high surface area and frontal area. So, concerning our second question, hatchlings have a higher drag coefficient than older larvae, and viscous drag is the main contributor to total drag in all age groups. The hydrodynamic scaling hypothesis is therefore also supported by the data.

Development of burst & coast swimming.

Concerning our third question 'which of the two hypotheses provides a better explanation', our experimental data show that hatchlings suffer almost equally from a low initial coasting speed and a low decay constant of their coasting speed compared with larvae aged 3 and older. Consistent with these kinematics data are our behavioral observations. The switch in swimming style occurs between age 2 (almost exclusively sustained swimming) and age 4 (almost exclusively burst & coast swimming), in good agreement with our data on coasting performance and drag.

Our data set overlaps with a previously published data set on zebrafish larvae of age 5 days. McHenry and Lauder [11, 15] evaluated the hydrodynamic scaling of zebrafish from age 5 days onwards. Their relevant values for decay constant (0.12 s) and drag coefficient (5.3) are very similar to our findings for larvae at age 5 dpf. They also conclude that coasting performance continues to improve as larvae get older due to improvements in the drag coefficient that are caused by the increasing streamlining of the fish.

Implications of flow patterns.

Osse and van den Boogaart [23] proposed that fish larvae might perform small bursts to replace the old, oxygen-depleted water in their boundary layer with fresh, oxygen-rich water. Our flow visualizations show that the larva might shed a smaller proportion of the boundary layer than originally assumed as the shed boundary layer catches up again with the larva during the coast.

Acknowledgments

We would like to thank de Haar Vissen for breeding and maintaining the zebrafish, Ansa Wasim for help with making the recordings, and Sander Kranenbarg for help with Matlab for the data analysis. UKM was funded by NWO-ALW grant 814.02.006 and a JSPS fellowship. This work (of HL) is partly supported by a PRESTO-JST program, and the Grant-in-Aid for Scientific Research of No. 18656056 and No. 18100002, JSPS, Japan. HL was also funded by a CKSP fellowship.

References

(1) Videler, J.J., Weihs, D., Energetic advantages of burst-and-coast swimming of fish at high speeds, *Journal of Experimental Biology* Vol. 97 (1982), pp.169-178.

(2) Alexander, R.M., Optimization and gaits in the locomotion of vertebrates, *Physiological Reviews* Vol. 69 (1989), pp.1199-1227.

(3) Weihs, D., Energetic advantages of burst swimming of fish, *Journal of Theoretical Biology* Vol. 48 (1974), pp.215-229.

(4) Batchelor, G.K., *An Introduction to Fluid Dynamics*, (1967), Cambridge University Press.

(5) Lamb, H., *Hydrodynamics*, (1945), 6th edition, Dover Publications.

(6) Fuiman, L.A. (2002). Special considerations of fish eggs and larvae. *Fishery Science: The Unique Contributions of Early Life Stages*, edited by L. A. Fuiman and R. G. Werner, pp.1-32, Blackwell.

(7) Fuiman, L.A., Webb, P.W., Ontogeny of routine swimming activity and performance in zebra danios (Teleostei: Cyprinidae). *Animal Behavior* Vol. 36 (1988), pp.250-261.

(8) Budick, S.A., O'Malley, D.M., Locomotor repertoire of the larval zebrafish: swimming, turning and prey capture. *Journal of Experimental Biology* Vol. 203 (2000), pp.2565-2579.

(9) Müller, U.K., van Leeuwen, J.L., Swimming of larval zebrafish: ontogeny of body waves and implications for locomotory development. *Journal of Experimental Biology* Vol. 207 (2004), pp.853-868.

(10) Fuiman, L.A., Batty, R.S., What a drag it is getting cold: partitioning the physical and physiological effects of temperature on fish swimming. *Journal of Experimental Biology* Vol. 200 (1997), pp.1745-1755.

(11) McHenry, M.J., Lauder, G.V., The mechanical scaling of coasting in zebrafish (*Danio rerio*). *Journal of Experimental Biology* Vol. 208 (2005), pp.2289-2301.

(12) Hunter, J. R., Swimming and feeding behavior of larval anchovy *Engraulis mordax*. *Fishery Bulletin* Vol. 70 (1972), pp.821-838.

(13) Fuiman, L.A., Burst-swimming performance of larval zebra danios and the effects of diel temperature fluctuations, *Transactions of the American Fisheries Society* Vol. 115, No.11 (1986), pp.143-148.

(14) Weihs, D., Energetic significance of changes in swimming modes during growth of larval anchovy, *Engraulis mordax*. *Fishery Bulletin* Vol. **77** (1980), pp.597- 604.

(15) McHenry, M.J., Lauder, G.V., Ontogeny of form and function: locomotor morphology and drag in zebrafish (*Danio rerio*), *Journal of Morphology* Vol. 267 (2006), pp.1099-1109.

(16) Woltring, H. J., A Fortran package for generalised, cross-validatory spline smoothing and differentiation. Advances in Engineering Software. Vol. 8, No.2 (1986), pp.104-113.

(17) Fontaine E., Lentink D., Kranenbarg S., Müller U.K., van Leeuwen J.L., Barr, A.H., Budick J.W., Automated visual tracking for studying the ontogeny of zebrafish swimming, *Journal of Experimental Biology* Vol. 211 (2008), pp.1305-1316.

(18) Hart, D.P., Super-resolution PIV by recursive local-correlation, *Journal of Visualization*, Vol. 10 (1999), pp.1-10.

(19) Müller U.K., van den Boogaart J.G.M. van Leeuwen, J.L., Flow patterns of larval fish: undulatory swimming in the intermediate flow regime, *Journal of Experimental Biology* Vol. 211 (2008),

pp.196-205.
(20) Aono, H., Liang, F., Liu, H, Near- and far-field aerodynamics in insect hovering flight: an integrated computational study, *Journal of Experimental Biology* Vol. 211 (2008), pp.239-257.
(21) Liu, H., Kato, N., A numerical study of unsteady hydrodynamics of a mechanical pectoral fin, *Journal of Bionetic Engineering*, Vol. 1, No.2 (2004), pp.108-120.
(22) Aono, H., Shyy, W., Liu, H., Vortex dynamics in near wake of a hovering hawkmoth, *AIAA Paper* 2008-0260, 2008.
(23) Osse, J.W.M. and van den Boogaart, J.G.M., Dynamic morphology of fish larvae, structural implications of friction forces in swimming, feeding and ventilation. *J. Fish Biol.* Vol. 55 (1999), pp.156-174.